CHAPTER-1

Introduction and literature survey

1. Introduction

The progressive advancement in the economy, industry, and population in the 21st century significantly relies on the utilization of the energy obtained from fossil fuels [1]. Fossil fuels mainly involve 34% petroleum, 27% coal, and 24% natural gas having a huge amount of carbon content [1]. It is projected that the total energy demand of the world will be 17,487 Mtoe (Million Tonnes of Oil Equivalent) in 2040 [2]. The highest energy demand will be from Africa and Asia will be the second for the consumption of primary energy [2]. Global energy consumption is believed to upsurge from 13.5 TW/year today to 27.6 TW per/year by 2050 and 43 TW/year by 2100 [3]. In recent days, fossil fuels contribute 85% of the total global energy consumption [1]. Several estimations have been presented for the long-time existence of fossil fuels and the percentage of the energy demand that will be fulfilled from fossil fuels. It is well known that the natural sources of fossil fuels are limited and are decreasing with time due to their increasing consumption. Fossil fuels generate 21.3 billion tons of carbon dioxide (CO_2) per annum because of the combustion of various energy resources [4]. CO_2 is one of the greenhouse gases, which is responsible for global warming and environmental pollution. Therefore, it is widely accepted that fossil fuels cannot be utilized as the primary source of global energy supply to avoid the above-mentioned problems and keep constant the present CO_2 level in the atmosphere [1].

In this regard, many countries have paid great efforts to obtain energy from renewable sources and reduce the generation of greenhouse gases by combustion of fossil fuels. As a result, the significant production of renewable energies has indeed increased. In this regard, the Paris Agreement was adopted in December 2015 as a legally enforceable international treaty on climate change [5]. For the first time, this is the only legal agreement, which inspires all the countries to make their efforts to fight climate change. The main goal of this agreement is to limit global warming below 2 ^{o}C in comparison to pre-industrial levels [5].

A body of the UN, the Intergovernmental Panel on Climate Change (IPCC) has been constituted for the scientific assessment of climate change [6]. In September 2019, the IPCC special report on climate change provides significant insights into the reduction of global warming to the lowest possible level following the goal of the 2015 Paris Agreement [6].

Further, European Union proposed a 2030 Climate Target Plan, which targets to reduce greenhouse gas emissions by at least 55% by 2030 compared to 1990 levels [7]. The main objective of the plan is to reduce emissions from industry, transport, and farming. This target will lead Europe to become climate neutral by 2050. In 2010, the government of Germany proposed an exciting plan "the *Energiewende*, i.e. an energy change or revolution" to reduce CO_2 generation by utilizing renewable sources [8]. As a result, one-third of the electricity consumed in the country was derived from renewable sources in 2015.

The government of India has also taken serious steps for the reduction of one billion ton cumulative carbon emissions by 2030. Also, India is targeting to achieve net zero carbon emission by 2070 [9]. The Ministry of Power (MoP) proposed Green Hydrogen

Policy. The National Hydrogen Mission targets of making India a platform for the production and export of green hydrogen.

Among all the proposed plans, the use of hydrogen (H_2) replacing fossil fuels purveys a long-lasting solution to address the global energy demand [10]. H_2 has a very high gravimetric energy density of 142 MJ kg^{-1}, which is three times larger than gasoline [11]. H_2 can be directly utilized in an engine or oxidized in a fuel cell producing H_2O as the product without CO_2 emission. The H_2 can be produced by biological, thermal, chemical, photocatalytic, and electrochemical methods. The strategies like coal gasification, reforming of natural gas, pyrolysis of biomass, dark fermentation process, and water electrolysis are also utilized for H_2 production [12].

Owing to the low cost, high energy efficiency, and eco-friendly environment, electrochemical energy conversion emerges as a promising route to produce clean, eco-friendly, and sustainable H_2. Electrochemical energy conversion involves the conversion of electrical energy into chemical energy, i.e. to store the energy in chemical bonds [13]. The thermodynamic efficiency of the electrochemical energy conversion processes is found to be better than any thermal cell working on the Carnot principle. Moreover, the integration of electrochemical energy conversion processes with solar cells can improve the efficiency of the system [14].

Nowadays, electrochemical water splitting has been widely accepted as a green and clean electrochemical energy conversion technology generating a carbon-free H_2 fuel [15]. In recent days, 3.9% of the total hydrogen is generated from water electrolysis [16]. Usually, the generated H_2 fuel is categorized into black H_2, blue H_2, and green H_2 [17]. Black hydrogen is obtained by the burning of coal. It is not eco-friendly because it produces a huge amount of CO_2 after burning coal. The generation of every ton of black hydrogen is accompanied by the emission of 10-12 tons of CO_2. Blue hydrogen is

produced by steam reforming. Although it is considered cleaner than black hydrogen, it also emits CO_2 during production. Further, green H_2, the only solution for clean and carbon-free energy, is produced by water electrolysis without the emission of harmful greenhouse gases. The combustion of green hydrogen leads to the generation of a huge amount of energy and water. Owing to the eco-friendly production and great potential for energy-related applications, significant attention has been provided to produce green hydrogen in the last ten years [17].

1.1. Electrochemical water splitting

Electrochemical water splitting is considered as an excellent energy conversion technology to generate green and eco-friendly hydrogen fuel [18]. Depending on the nature of the electrolyte, operating conditions, and the electrocatalysts, alkaline water splitting and proton exchange membrane (PEM) water splitting are utilized for the production of H_2 [19]. First, Troostwijk and Diemann introduced alkaline water splitting in 1789. Further, Grubb in 1950 and the General Electric Co. developed PEM water electrolysis for the first time [19].

The PEM water electrolyzer has been recorded to achieve high current densities ~2 A cm^{-2} while the alkaline water electrolyzer produces comparatively low current density. The PEM water electrolyzer requires precious metal-based catalysts [19] while alkaline water splitting has the benefits of using low-cost transition metal-derived catalysts to attain 70%–80% commercialization energy efficiency. However, it suffers from the high input of potential and sluggish kinetics. Electrochemical water splitting is a thermodynamically-uphill process demanding an energy input of 237.1 kJ mol^{-1} [20].

Electrochemical water splitting is the splitting of water molecules into hydrogen (H_2) and oxygen (O_2) by electrolysis (Figure 1.1) [21]. The two complementary reactions of water splitting are observed to happen at the cathode (hydrogen evolution reaction-HER)

and anode (oxygen evolution reaction-OER). The reaction mechanisms of the OER and HER are largely affected by the pH of the electrolyte. The HER is efficient in acidic electrolytes because of the abundant protons whereas the OER shows high efficiency in the alkaline medium due to the presence of the excess amount of hydroxyl ions [22]. The HER is a two-electron transfer process, which is accompanied by the involvement of potential 0 V *vs* RHE [23].

As HER is more favorable in the acidic medium, carrying out the reaction in the alkaline electrolyte imposes an extra step for the dissociation of water molecules to protons leading to the slow reaction kinetics. As a result, the HER in alkaline medium requires high potential compared to the acidic electrolyte. Two different mechanisms (Volmer-Heyorvsky and Volmer-Tafel) are involved in the HER depending on the pH of the electrolyte [24,25].

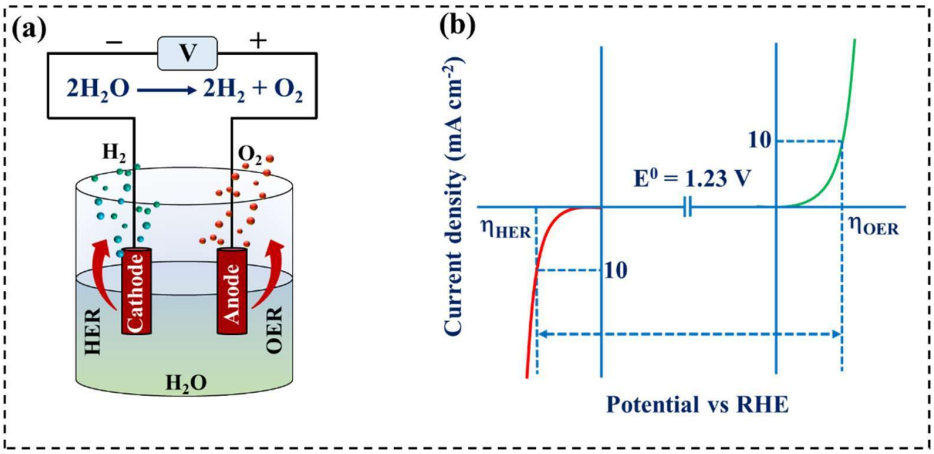

Figure 1.1. (a) Schematic depiction of the electrochemical water splitting showing anodic OER and cathodic HER and (b) plot of the potential *vs* current density for OER and HER.

In contrast, the anodic OER involves the formation of O-O bond to produce O_2 by the oxidation of water [26]. The overall efficiency of electrochemical water splitting depends on the anodic OER. The generation of high-energy reaction intermediates during the OER

creates a high kinetic energy barrier. As a result, the kinetics of OER becomes slow and it requires high energy in the form of overpotential [22,27–30]. As the water splitting is affected by the change of the pH of the electrolyte, the OER follows significantly different pathways in alkaline and acidic electrolyte.

Initially, H_2O is observed to be coordinated with the surface active sites with simultaneous proton and electron transfer producing surface M-OH species. Further, the proton-coupled oxidation of the surface active site or disproportionation of two M-OH species results in the generation of M-O species. The decomposition of M-O species occurs either by coupling or by the attack of H_2O (or OH^-) to form O-O bond and releases O_2 [31–35].

The previous studies have shown a standard free energy change (ΔG) of 4.92 eV for anodic OER. As a result, each elementary step for the formation of *OH, *O, *OOH, and O_2 is accompanied by ΔG of 1.23 eV (4.92/4 = 1.23 eV) [30,36–38]. However, an extra energy (overpotential) over 1.23 eV is required for a real catalyst to proceed with the overall process. In this regard, a huge number of electrocatalysts have been demonstrated for the electrochemical OER to reduce the extra energy demand and accelerate the reaction kinetics [39,40,49,41–48]. The electrocatalysts designed for electrochemical OER can be assessed based on the activity, kinetics, and stability.

1.2. Parameters of electrochemical water splitting

As the electrochemical OER is a kinetically slow and thermodynamically uphill reaction, efficient electrocatalysts are employed to reduce the required overpotential as well as fasten the reaction kinetics. The performance of an electrocatalyst can be analyzed for electrochemical OER based on the following parameters:

1.2.1. Overpotential (η)

The overpotential is known as the most important parameter, which defines the catalytic

activity of an electrocatalyst [50–55]. The overpotential is defined as the extra potential required to drive an electrochemical process from its reversible potential (Figure 1.2a) [54–57]. Hence, the overpotential for OER at a defined current density can be calculated using the equation $\eta_{OER} = (E_{RHE} - 1.23)$ V [54–57]. It should be mentioned here that the electrocatalyst, which requires low overpotential, will be more active. Generally, the geometric current density of 10 mA cm^{-2} is considered as the benchmark to compare the overpotentials (i.e. catalytic activities) of the various electrocatalysts. In several cases, the electrocatalyst with high mass loading represents the overpotential at the current densities of 50 and 100 mA cm^{-2} [58–61].

The concept of *iR* compensation for polarization curves has been introduced as most of the electrocatalytic activities are evaluated in a three-electrode cell, where the solution resistance (R_s) is high [54,55]. Therefore, the *iR* drop compensated potential with the determined R_s is considered as the actual overpotential of an electrocatalyst required for OER. The *iR* drop compensated overpotential can be determined as:

$$\eta_{OER} = (E_{RHE} - 1.23 - E_{iR})\ V$$

1.2.2. Tafel slope

The analysis of the Tafel slope is one of the primary parameters for the evaluation of the reaction kinetics of electrochemical OER (Figure 1.2b) [62,63]. Generally, the Tafel slope is calculated from the Tafel equation as given below [54,55]:

$$\ln J = \ln J_0 + (\alpha_A nF/RT)\eta$$

The plot of log J *vs* η results in the slope $(d\log J/d\eta) = (2.303RT/\alpha_A nF)$ (Where, J = current density, η = overpotential, R = gas constant, T = temperature, α_A = charge transfer coefficient, n = number of electron transferred, F = Faraday constant. This slope is known as the Tafel slope (Figure 1.2b). It is clear that the Tafel slope is inversely proportional to the charge transfer coefficient (α) [54,55]. As a result, the lower Tafel slope is observed

to show faster charge transfer properties indicating the faster OER kinetics. Due to the involvement of many steps in OER, the type of mechanism cannot be determined from the Tafel plots. However, the number of electrons transferred during OER can be calculated for the related electrocatalyst.

1.2.3. Stability

The stability of an electrocatalyst for electrochemical OER can be evaluated either by chronoamperometry (CA) or chronopotentiometry (CP) [64,65]. The CA is defined as the monitoring of the current density produced by an electrocatalyst with the time at a fixed applied potential (Figure 1.2c) [66–70]. Generally, the transition metal-based electrocatalysts show excellent stability without any loss of current density for days under CA conditions. On the other hand, CP is known as the monitoring of the generated potential with time at a fixed current density [66,71,72]. Here, the current density of 10, 20, 50 or 100 mA cm^{-2} can be selected to demonstrate the stability of an electrocatalyst. Further, cyclic voltammetric stability is also determined to assess the overall stability of an electrocatalyst. The active electrocatalyst should possess the highest possible cyclic stability without loss of overpotential and current density.

1.2.4. Electrochemical surface area (ECSA)

In general, most of the reports of electrochemical water splitting use the geometrical surface area as the important parameter, which is considered the area of the electrodes for a smooth and planar surface [54,73]. Later, the term ‘‘real surface area’’ was introduced using Brunauer–Emmett–Teller (BET) isotherm based on the adsorption and desorption of N_2 gas [54,73]. However, all the surface sites which are active for adsorption and desorption of N_2 molecules cannot be active for electrochemical reactions [54,73].

As electrochemical water splitting is a surface phenomenon, the term electrochemical surface area (ECSA) is more useful to understand the phenomenon. The ECSA is defined

as the surface area, which is exposed to the electrolyte for the electrochemical reactions [54,73]. The ECSA depends on the mass loading, structure, morphology, and properties of an electrocatalyst under study. Generally, the few layers of the surface participate in electrochemical reactions. As a result, the mass loading significantly affects the ECSA. The catalytic activity normalized by ECSA gives meaningful information about the intrinsic activity of the electrocatalysts, which have different sizes, shapes, morphology, topography, and porosity [74–77]. The ECSA of an electrocatalyst can be evaluated by various methods in which the double layer capacitance (C_{dl}) measurement method has been widely used (Figure 1.2d) [78–80]. For the determination of the ECSA, the C_{dl} of the material is determined using CV in the non-faradaic region. Further, the ECSA is calculated based on the following formula [81,82]:

$$\text{ECSA} = C_{dl}/C_s$$

The C_s is the specific capacitance of the material [81,82]. The larger ECSA of an electrocatalyst promotes catalytic activity due to the presence of a large number of surface active sites.

1.2.5. Number of active sites (Γ)

The number of active sites is an important parameter for water splitting [54,55,83]. Generally, the metal centers of an electrocatalyst undergo *in-situ* oxidation and reduction before the onset of OER [64,65,82,84,85]. Moreover, the metal sites, which are *in-situ* oxidized or reduced during the electrochemical process, are assumed to participate in OER. Therefore, the number of surface active sites of the electrocatalysts can be calculated by the integration of the peak area of the redox peak(s) for the *in-situ* oxidation or reduction to form (oxy)hydroxide (Figure 1.2e) [64,65,82,84,85]. The area of the redox peak is integrated and divided by the scan rate to get the associated charge [86]. Further, the associated charge is divided by the number of electrons transferred during the *in-situ*

oxidation or reduction of metal sites to obtain the number of surface active sites participating in OER.

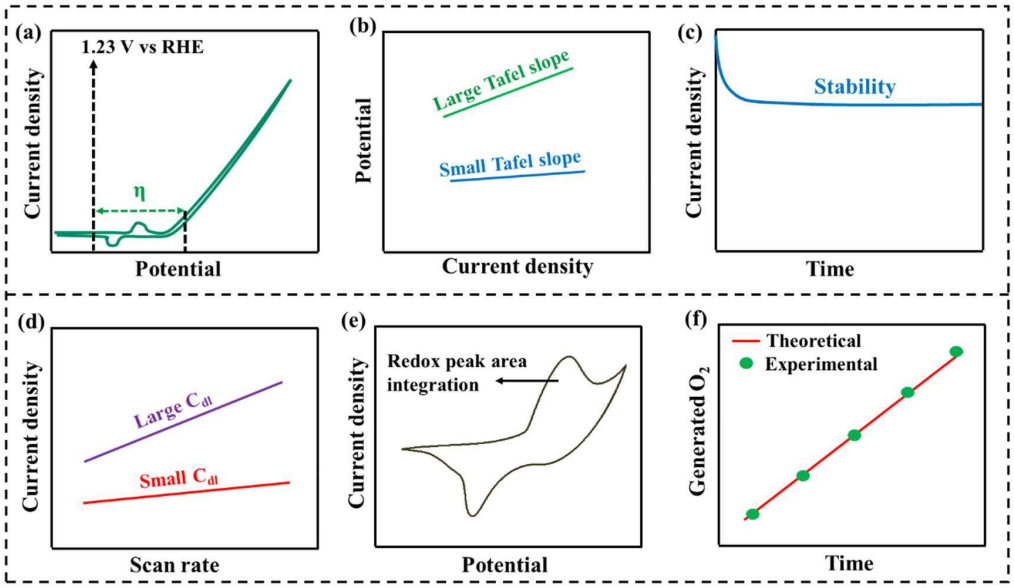

Figure 1.2. (a) Cyclic voltammetry profile for OER; (b) Tafel plots of the electrocatalysts for OER; (c) CA stability test of an electrocatalyst for OER; (d) C_{dl} plot for the calculation of ECSA; (e) CV profile showing the redox peak for the determination of surface active sites of an electrocatalyst and (f) plot for the faradaic efficiency measurement.

1.2.6. Turn-over frequency (TOF)

TOF is another activity parameter, which is determined to get more insights into the intrinsic activity of an electrocatalyst [65,85,86]. TOF of an electrocatalyst cannot be influenced by the mass loading, shape, size, and morphology of the catalyst reflecting the intrinsic activity. TOF can be calculated from the current density at a fixed potential and the number of surface active sites involved in the electrochemical process [54,55]. The electrocatalyst which has the highest TOF reflects the highest intrinsic activity for the

electrochemical process. The TOF can be determined by the following formula [54,55,87,88]:

$$TOF = (J \times N_A)/(n \times F \times \Gamma)$$

Where J denotes the current density at a fixed potential, N_A is the Avogadro number, n is the number of electrons transferred during the electrochemical process, F represents the Faraday constant, and Γ denotes the number of surface active sites.

1.2.7. Faradaic efficiency (FE)

Faradaic efficiency (FE) of an electrocatalyst is determined to explain the utilization of charges in the production of O_2 and H_2 [54–57]. The FE can be calculated by comparing the experimentally measured quantity of the evolved gas and the theoretically calculated amount of gas based on Faraday's laws (Figure 1.2f) [89–92]. The most widely accepted method for the determination of FE is the water-gas displacement method. In this method, the volume of the evolved gas is collected in a jar by water displacement and then converted into moles using Avogadro's principle [69,93]. Further, the theoretical moles of the gas molecules are determined from the charge passed during the electrolysis using Faraday's second law of electrolysis. When the evolved moles and theoretically calculated moles of gases are in agreement, 100% FE is observed for the studied electrocatalyst [89–92]. This indicates that the catalyst is highly selective for that electrochemical reaction ensuring no involvement of the other side reactions.

1.3. Electrocatalysts for oxygen evolution reaction (OER)

The electrocatalysts employed for OER reduce the overpotential and accelerate the reaction kinetics [31,94]. Generally, the noble metal-based RuO_2 and IrO_2 have been utilized with high activity and stability for OER in the acidic medium [95–98]. Moreover, Ru, Ir, Rh based alloys have also been explored to attain efficient OER [99–101]. In contrast, the OER activity of RuO_2 and IrO_2 in an alkaline medium is not up to the

practical mark. However, the high price and rare earth abundance of noble metals hamper their practical application on a large scale [84,102–106]. In this regard, transition metal-derived catalysts like metal oxides, hydroxides, phosphides, selenides, sulfides, etc., have been explored recently with proficient electrochemical activity and stability for OER [107–135].

1.4. Electrochemical reconstruction of transition metal-based precatalysts

A precatalyst can be defined as a precursor, which can be transformed into an active OER catalyst under oxidizing anodic conditions [44,136–139]. The transition metal-based electrocatalysts do not work as the real catalyst rather they are oxidized under harsh anodic conditions in the alkaline electrolyte to form metal hydroxide-(oxy)hydroxide [$M(OH)_2$-M(O)OH], which is considered as the real catalyst for OER [64,137,138,140–145]. A series of electrochemical processes occur during the electrochemical OER with transition metal-based electrocatalysts such as structural reconstruction, morphological transformation, and compositional and electronic structure modulation [21,40,150–152,65,103–105,146–149].

It has been observed that the metal centers of transition metal-based catalysts are *in-situ* oxidized before OER because of the high applied potential of more than 1.4 V *vs* RHE [21,40,150–152,65,103–105,146–149]. The oxidation of metal centers to their higher oxidation state (M^{3+}/M^{4+}) takes place under the anodic potential in alkaline electrolytes. Consequently, the attack of hydroxyl ions and water molecules under the applied potential renders $M(OH)_2$-M(O)OH active catalyst [136,137,144]. Most of the previous reports have indicated the electrochemical reconstruction of the precatalysts by CA methods [64]. However, the CV activation method is also employed for the electrochemical reconstruction of the precatalyst to generate the active catalyst [64].

1.4.1. Surface reconstruction

The surface of most electrocatalysts is changed under the anodic conditions during the OER process leading to a newly reconstructed surface [106,117,153–157]. Mostly, transition metal-derived electrocatalysts undergo surface reconstruction in electrochemical conditions to produce an $M(OH)_2$-M(O)OH layer on their surface (Figure 1.3a) [44,105,118,158–160]. The electrochemical surface reconstruction of oxides [140,161,172], phosphides [143,146], sulfides [143], selenides [173] etc. have been well established with spectroscopic and microscopic characterizations [174–177]. During the reconstruction process, structural transformation, surface oxidation, ion leaching, morphological changes, and composition tuning occur under the applied anodic potential [64,65,84,86].

The applied anodic potential, electrolyte pH, temperature, atmosphere, and pressure have a significant influence on the surface reconstruction of the precatalysts [64]. Generally, the high anodic potential and alkaline electrolyte promote the surface reconstruction while in some cases under high anodic potential, the complete reconstruction of the precatalysts has also been observed [103,136,138,151,156,161-163]. The main evidence for the morphological changes is obtained through TEM studies. After the surface reconstruction, an obvious amorphous or crystalline layer of $M(OH)_2$-M(O)OH is observed in TEM images [143,144]. The PXRD is used to realize the crystalline or amorphous nature of the $M(OH)_2$-M(O)OH layer [64,104,152].

Generally, preferential dissolution of metals or anions from the precatalyst and the incorporation of metal ions from the electrolyte takes place during the reconstruction process [140,156,164,165]. Therefore, EDX and ICP studies are performed to determine the compositional changes after the surface reconstruction. The XPS studies have been employed to detect the changes in oxidation states and electronic properties of the

elements after reconstruction [46,136,166–168]. The XPS studies confirm the existence of high valent metal ions with metal-oxygen bonds in the reconstructed active catalysts. Further, the tuning of coordination properties during the reconstruction is determined using *in-situ* XAS and Raman spectroscopy [52,59,105,132,169–171].

1.4.2. Bulk reconstruction

In contrast to surface reconstruction, the implementation of meta-stable materials for anodic OER leads to bulk electrochemical reconstruction [82,178–183]. For example, when meta-stable metal-organic frameworks (MOFs) like BDC-MOF, ZIF, and PBA, have been used as the precatalysts for anodic OER, they are completely reconstructed into active $M(OH)_2$-M(O)OH catalysts under the effect of applied potential (Figure 1.3b). [82,178–183].

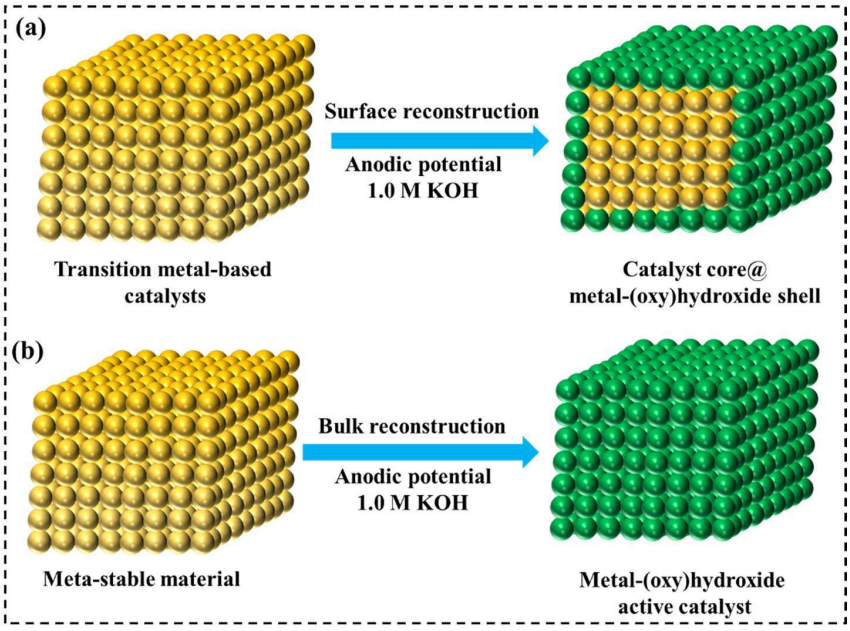

Figure 1.3. (a) Electrochemical surface reconstruction of transition metal-based precatalysts to form catalyst core and metal-(oxy)hydroxide shell and (b) electrochemical bulk reconstruction of meta-stable materials to form ultrathin metal-(oxy)hydroxide active catalyst.

The bulk reconstruction is accomplished by the complete change of morphology, phase, composition, and electronic structure [82,178–183]. The anodic potential-driven metal-ligand destruction, leaching of ions, oxidation of metal centers, hydroxylation, and hydration of MOFs render the ultrathin $M(OH)_2$-M(O)OH nanosheets having atomic-level thickness [61,82,139,178–183]. The nanosheets provide a large electrochemical surface area, accessible active sites, and improved charge and mass transport compared to the pristine MOFs. Hence, the catalytic performance of active $M(OH)_2$-M(O)OH catalyst is found to be superior to the pristine MOFs.

1.5. Metal-organic framework (MOF) as precatalyst

MOFs can be defined as porous 3D crystalline materials constructed by metal ions and organic linkers [29,196–200][13,184]. In 1943, crystalline materials were reported using metal centers, and nitrogen organic linkers, known as Werner-type complexes [185]. In the 1960s, various coordination compounds like Hofmann-type clathrate were investigated by Iwamoto and co-workers [186]. A coordination polymer denoted by the formula $Ni(NH_3)_2(CN)_4(C_6H_6)$ was first prepared by K.A. Hofmann [186,187].

Further, Omar M. Yaghi and co-workers developed the first robust and highly porous material named MOF-5 [188]. The term metal-organic framework was first coined in 1995 [188]. From 2002 onwards, a series of MOFs have been prepared using a variety of 1,4-benzenedicarboxylic acid (BDC), other dicarboxylic acids, and functional groups like phenols, alkyl amines, thiols, etc [189-191]. In further progress, MOFs like ZIF, PB, PBA, etc. have been prepared successfully by using various metal ions [28,59,192–195]. The major advantages of MOFs include their high porosity, designed morphology, desired composition, large surface area, and large number of active sites. Moreover, fine-tuning of the structural and electronic properties and easy and facile synthesis also provide several benefits. As MOFs can be shaped in various morphologies, they possess

high porosity with enormous surface areas and void spaces [29,196–200]. Several mesoporous and microporous MOFs have been developed where the void spaces in MOFs vary from a few Ångströms to tens of nanometers [201–204].

The versatility of MOFs is observed due to their easier synthesis from the different combinations of metal ions and organic linkers. As a result, an infinite number of MOFs can be designed with varying sizes, shapes, and porosity, which can also be tuned by the length, geometry, and functional groups of the organic linkers [205–208]. In addition, the geometry, hydrophilicity, hydrophobicity, acidity, basicity, and functionality of MOFs can also be tailored [205–208].

MOFs have been widely explored for various applications in the field of gas sorption, removal of radioactive elements, biomedicine to cancer therapy, supercapacitors, and lithium and sodium ion batteries [209–213]. Although MOFs furnish unique structural and electronic properties, the direct implementation of MOFs for electrochemical OER is rarely studied due to their low electronic conductivity, poor mass permeability, and low stability under electrochemical conditions [29,64,82]. However, this instability of MOFs can be utilized by introducing the MOFs as the precatalysts for electrochemical reconstruction [29,64,82]. This leads to the bulk reconstruction of MOFs into ultrathin $M(OH)_2$-M(O)OH nanosheets [29,64,82]. The bulk reconstruction involves hydroxylation, hydration, anodic oxidation, and self-assembly (Figure 1.4).

1.6. Prussian blue (PB) and Prussian blue analogues (PBAs)

Prussian blue (PB) belongs to a subclass of MOFs, where the coordination of metal ions with the –CN bridges demonstrates a polymeric structure [214,215]. Prussian blue ($Fe_4[Fe(CN)_6]_3$) was discovered accidentally by a paint maker Diesbach in Berlin in 1704 [216]. PB is the first coordination polymer artificially synthesized by the co-precipitation of Fe^{III} salt and $[Fe^{II}(CN)_6]^{4-}$ [217]. Further, progress in the field of PB leads to the

substitution of the Fe atom by other metal ions like Mn, Co, Ni, Cu, Zn, etc. resulting in the formation of similar structures termed as Prussian blue analogues (PBAs) (Figure 1.5) [214,215]. The PBAs are denoted by the formula $A_m[B_n(CN)_x]_y.zH_2O$ (where A, B = Mn, Co, Ni, Cu, Zn etc. and z = 6-14) [218,219].

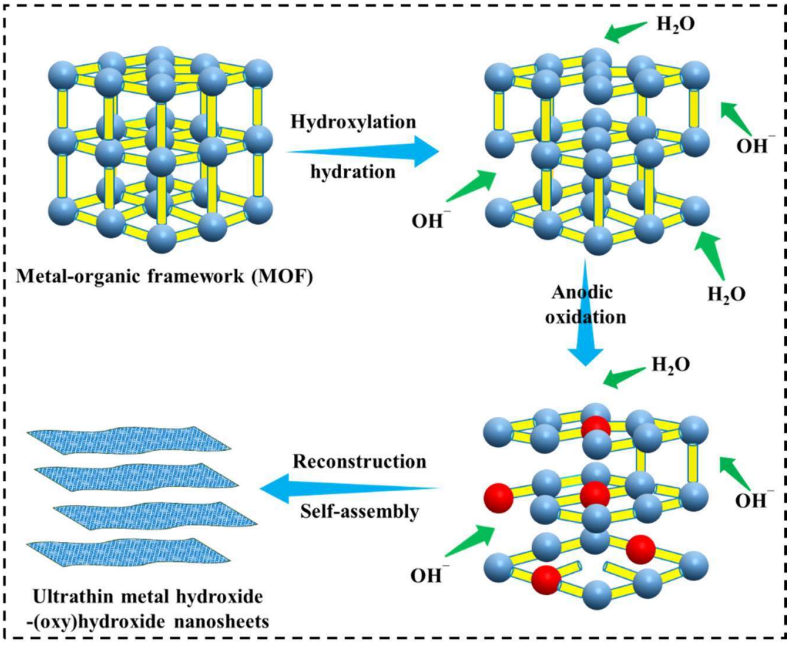

Figure 1.4. Schematic depiction for the electrochemical bulk reconstruction of MOFs into ultrathin metal hydroxide-(oxy)hydroxide nanosheets.

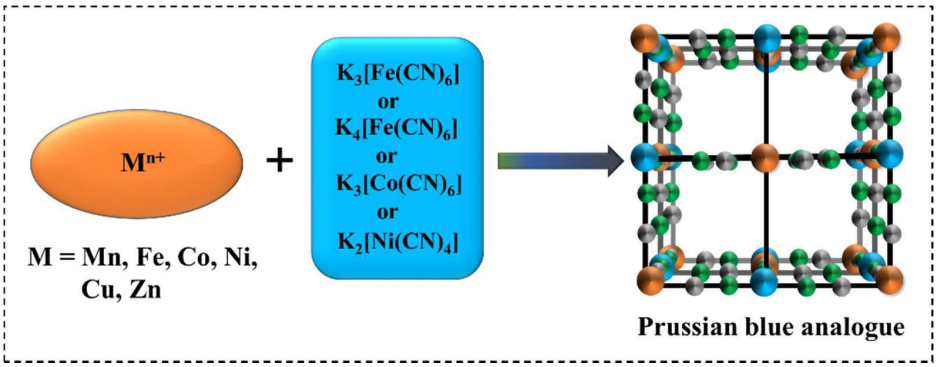

Figure 1.5. Designing of PBAs using different metal ions and cyanometalate reagents, color code: brown and sky blue colored spheres denote the metal centers while grey and green colored spheres denote the carbon and nitrogen atoms, respectively.

Similar to the PB, the nitrogen atoms of the cyano bridges are connected to the metal ions of A sites and the carbon atoms are coordinated to the metal ions of B sites in PBAs. Most of the PBAs possess the face-centered cubic crystal system having space group *Fm3m* [218,219]. However, the hexagonal crystal system has also been reported with space group R-3c in some cases [218,219]. Owing to their large surface area, highly porous structure, exposed facets, desired composition, and tunable electronic properties, PBAs have been employed in various applications like batteries, supercapacitors, etc.

1.7. PBA as precatalyst for electrochemical water oxidation

Although various applications of PBAs have been investigated in recent years, their application in electrochemical water splitting has been rarely explored [21,29,64]. The poor electronic conductivity, low electron transfer due to –CN bridges, low mass transport, and instability under electrochemical conditions are the factors obstructing the direct implementation of PBAs in electrochemical water splitting [21,29,64]. As a result, there are very few reports on the direct application of PBAs in electrochemical water splitting. Interestingly, PBAs are observed to undergo the complete bulk electrochemical reconstruction process driven by the applied potential to form active $M(OH)_2$-M(O)OH catalysts (Figure 1.6) [21,29,64].

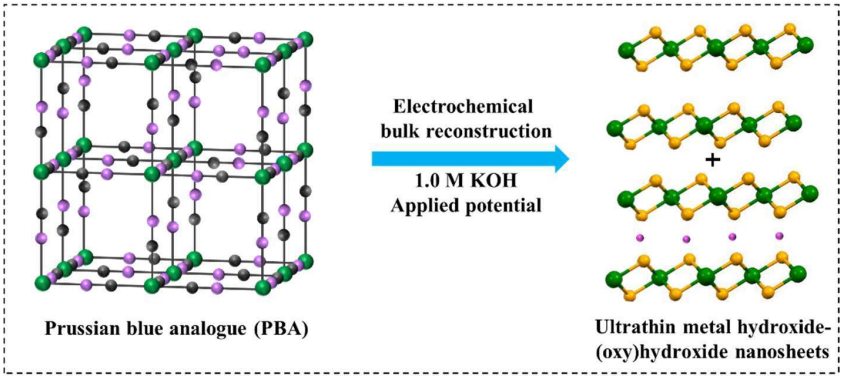

Figure 1.6. Formation of ultrathin metal hydroxide-(oxy)hydroxide nanosheets by the electrochemical bulk reconstruction of Prussian blue analogues.

The metal-cyanobridged structure of PBA is destroyed due to the hydroxylation and hydration process producing $M(OH)_2$ species. Further, the anodic oxidation of metal ions occurs to form M^{3+} centers. These M^{3+} centers undergo deprotonation under the effect of anodic potential generating a mixed phase of $M(OH)_2$-M(O)OH active catalyst [21,29,64].

In 2016, Galan-Mascaros group reported CoFe-PBA on FTO by cobalt hydroxide carbonate template route [220]. They employed CoFe-PBA for OER in acidic, neutral, and alkaline medium. They showed that the CoFe-PBA was stable in acidic (pH = 1) and neutral medium (pH = 7). However, they mentioned that "*At pH 14, CoFe is unstable and decomposes, probably to an oxo/hydroxo derivative*" [220]. In 2017, Indra et al. developed self-supported CoCo-PBA on carbon cloth using a cobalt hydroxide carbonate template for OER in alkaline medium [81]. They observed that CoCo-PBA@CC was not stable under oxidizing anodic conditions in alkaline medium and electrochemically reconstructed into Co(O)OH nanosheets.

Further in 2018, Su et al. investigated the bulk reconstruction of NiFe-PBA by CA in alkaline conditions [180]. The PBA was transformed into amorphous nickel hydroxide as the active catalyst after the electrochemical reconstruction. The active $Ni(OH)_2$ exhibited an impressively low overpotential of 258 mV affording a current density of 10 mA cm^{-2}. They performed operando X-ray spectroscopic studies, which revealed the anodic oxidation of *in-situ* generated $Ni(OH)_2$ into Ni(O)OH by the potential-dependent deprotonation process. Further, in 2019, bulk reconstruction of CoFe-PBA was demonstrated by Zhou et al. [179]. They employed the CA transformation of CoFe-PBA at 1.5 V forming Co(O)OH nanosheets. The hydroxylation and hydration of the CoFe-PBA resulted in the destruction of the framework by leaching of Fe and metal ion

oxidation. This ultimately formed Co(O)OH active nanosheets, which showed remarkable OER activity at 253 mV overpotential delivering 10 mA cm^{-2} current density.

The bulk reconstruction of PBAs into active $M(OH)_2$-M(O)OH catalysts results in high-quality nanosheets with transparent nature and optimum inter-layer distance [81,179,180]. The *in-situ* generated ultrathin nanosheets possess atomic level and uniform thickness leading to the large surface area and accessible active sites. The leaching of metal ions during the reconstruction creates structural defects with cationic vacancies [82,179,180]. Moreover, the anodic oxidation of M^{2+} ions results in the active catalysts with M^{3+}/M^{4+} ions, which makes the O-O bond formation easier.

Owing to these structural, morphological, and electronic properties, the electrochemically reconstructed $M(OH)_2$-M(O)OH nanosheets exhibit remarkable electrochemical performance and stability compared to ultrathin nanosheets prepared by hydrothermal or exfoliation method [64]. In most cases, powder forms of PBA precatalysts have been fabricated on solid supports like CC, and NF using a binder Nafion [11,29]. The utilization of binder fabricated precatalysts under applied potential for OER leads to the peeling of the catalyst from the electrode surface [11]. This ultimately deteriorates the catalytic activity and stability of the active catalysts and hence the activity is not up to the practical mark.

Looking at the above-mentioned issues, in this thesis, we have used self-supported PBA precatalysts on solid supports like CC, and NF by the metal hydroxide template route without the use of any binder. The electrochemical reconstruction of the self-supported PBAs renders the active $M(OH)_2$-M(O)OH catalysts on CC, NF. These *in-situ* generated self-supported $M(OH)_2$-M(O)OH catalysts exhibit outstanding catalytic activity and long-term stability.

1.8. Objectives of the thesis

As mentioned in the previous section, there is only one report for the direct implementation of self-supported PBAs for the electrochemical reconstruction to form active $M(OH)_2$-M(O)OH catalysts. However, the effect of the structure of the PBA on the electrochemical transformation process as well as on the active catalyst has never been studied. A systematic study to realize the effect of precatalyst structure, applied potential, and time to attain an efficient active catalyst is also missing in the literature.

To address these points, we have developed a series of self-supported CoFe-based PBAs on solid supports like CC, and NF (Table 1.1). The self-supported PBAs have been used as the precatalysts for the electrochemical transformation by applying anodic potential under CV and CA conditions. The electrochemical transformation results in the formation of a series of self-supported Fe-$Co(OH)_2$-Co(O)OH nanosheets (Table 1.1). The electrochemically reconstructed active catalysts have been employed for electrochemical OER, HER, and overall water splitting. The specific objectives of this thesis are listed below (Figure 1.7).

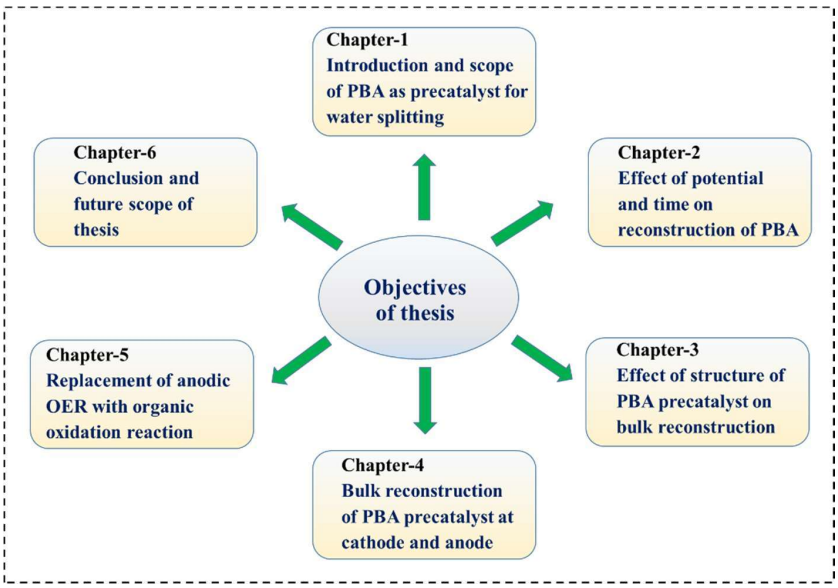

Figure 1.7. Diagram showing the chapter-wise specific objectives of the thesis.

(i) The self-supported PBA precatalysts have been demonstrated by the metal hydroxide template route. The anodic potential-driven electrochemical reconstruction of the PBA precatalysts has been performed under CA conditions producing a series of active Fe-$Co(OH)_2$-Co(O)OH catalysts. The potential and time for the CA reconstruction have been varied to demonstrate the effect on the structure, morphology, and activity of the active catalysts. Moreover, the best reaction condition for the synthesis of active Fe-$Co(OH)_2$-Co(O)OH catalyst has been investigated to achieve excellent water oxidation activity. The superiority of the reconstructed active catalysts over hydrothermally prepared CoHC@CC and CoFe-LDH@CC as well as noble metal-based RuO_2 catalysts has been demonstrated.

(ii) In further progress, we have attempted to modulate the structural and electronic properties of PBA precatalysts. Two different PBA precatalysts have been developed by varying the cyanometalate reagent. Further, the CV has been employed for the complete reconstruction of PBA precatalysts into active catalysts. The effect of structure, coordination, and electronic properties of PBA precatalysts on electrochemical reconstruction as well as on the structure, coordination, and electronic properties of the active catalysts has been confirmed from the spectroscopic investigations. The structure and activity factors have been successfully demonstrated with the XAS studies.

(iii) To achieve our next objective, the self-supported Fe-doped CoFeCo-PBA@CC has been synthesized by using a cobalt iron hydroxide template. For the first time, we have implemented the PBA precatalyst for the electrochemical anodic and cathodic reconstruction. The properties of the active catalysts at the cathode and anode have been examined by spectroscopic and microscopic studies. The effect of Fe introduction on the anodic and cathodic catalyst as well as on the water splitting activity has been demonstrated. For the first time, we have implemented the reconstructed catalysts for overall water splitting activity in a two-electrode electrolyzer.

Table 1.1. Details of the synthesized self-supported PBA precatalysts and corresponding electrochemically reconstructed active catalysts.

Precatalyst	Denoted name	Reaction condition	Active catalyst	Denoted name
Chapter-2				
CoFe-PBA@CC	PC-1	1.55 V, 12 h CA	Fe-$Co(OH)_2$-Co(O)OH@CC	AC-1
CoFe-PBA@CC	PC-1	1.45 V, 12 h CA	Fe-$Co(OH)_2$-Co(O)OH@CC	AC-2
CoFe-PBA@CC	PC-1	1.65 V, 12 h CA	Fe-$Co(OH)_2$-Co(O)OH@CC	AC-3
CoFe-PBA@CC	PC-1	1.55 V, 24 h CA	Fe-$Co(OH)_2$-Co(O)OH@CC	AC-4
Chapter-3				
CoFe-PBA@CC	PC-2	1-2 V, 600 CV cycles	Fe-$Co(OH)_2$-Co(O)OH@CC	AC-5
CoFe-PBA@CC	PC-3	1-2 V, 15 CV cycles	Fe-$Co(OH)_2$-Co(O)OH@CC	AC-6
Chapter-4				
CoFeCo-PBA@CC	PC-4	-0.2 V, 50 h CA	Fe-$Co(OH)_2$ @CC	AC-7
CoCo-PBA@CC	PC-5	-0.2 V, 50 h CA	$Co(OH)_2$@CC	AC-8
CoFeCo-PBA@CC	PC-4	1.50 V, 50 h CA	Fe-$Co(OH)_2$-Co(O)OH@CC	AC-9
CoCo-PBA@CC	PC-5	1.50 V, 50 h CA	$Co(OH)_2$-Co(O)OH@CC	AC-10
Chapter-5				
CoFe-PBA@NF	PC-6	1-2 V, 200 CV cycles	Fe-$Co(OH)_2$-Co(O)OH@NF	AC-11
CoCo-PBA@NF	PC-7	1-2 V, 200 CV cycles	$Co(OH)_2$-Co(O)OH@NF	AC-12

(iv) An attempt has been made to replace the kinetically sluggish anodic OER with the electrocatalytic benzyl alcohol (BA) oxidation reaction at a lower potential. The self-supported PBAs@NF have been transformed into an active Fe-$Co(OH)_2$-Co(O)OH@NF catalyst using the CV method. The improvement of the overpotential current density as well as H_2 evolution efficiency has been demonstrated by coupling the anodic BA oxidation reaction with HER. The formation of value-added benzoic acid at the low potential of 1.5 V *vs* RHE without the occurrence of OER has been investigated. The

effect of Fe doping in ultrathin $Co(OH)_2$-Co(O)OH catalyst on the activity and conversion of BA into benzoic acid has been established. The superiority of PBA-derived ultrathin nanosheets over hydrothermally prepared CoFe-LDH@NF has been analyzed for BA oxidation.